Materials Today Nano 21 (2023) 100266

Contents lists available at ScienceDirect

Materials Today Nano

journal homepage: https://www.evise.com/profile/#/MTNANO/login

Liquid cell scanning transmission electron microscopy characterization of combined chemical and electrochemical reduction of palladium

A.C. Meng [a, b, *], R. Serra-Maia [b], K.-B. Low [c], H. Lang [c], E.A. Stach [b, d, **]

[a] Department of Physics and Astronomy, University of Missouri, Columbia, MO 65211, USA
[b] Department of Materials Science and Engineering, University of Pennsylvania, Philadelphia, PA, 19104, USA
[c] BASF Corporation, Iselin, NJ, 08830, USA
[d] Laboratory for Research on the Structure of Matter, University of Pennsylvania, Philadelphia, PA, 19104, USA

ARTICLE INFO

Article history:
Received 12 July 2022
Received in revised form
27 August 2022
Accepted 11 September 2022
Available online 9 November 2022

Keywords:
Liquid cell TEM
Electrochemistry
Palladium
Ascorbic acid

ABSTRACT

We systematically investigate the effect of the driving force on the growth of palladium nanoparticles by comparing electrochemical reduction of polyvinylpyrollidone-stabilized palladium nitrate solution with chemical reduction by ascorbic acid using *in-situ* liquid cell transmission electron microscopy. Electrochemical data is simultaneously collected while high spatial resolution is maintained. As a chemical reductant, ascorbic acid results in the formation of smaller, more tightly spaced palladium nanoparticles through increased nucleation. When present during electrochemical reduction of palladium, ascorbic acid reduces the degree to which dendrites form due to the growth of a more compact palladium layer. Because the nanoparticles formed during chemical reduction have diameters on the order of a nanometer and are invisible under full liquid conditions, we employ electrochemical water splitting to generate a gas bubble in order to observe the process in real time. This is a step towards real-time characterization of complex solution-phase growth in which multiple pathways exist for metals to reduce and combinations of additives interact to control size and shape.

1. Introduction

The morphology of metallic nanostructures through solution-phase growth processes can be controlled both chemically and electrochemically. There can be additional components in the liquid, including chemical stabilizers, capping agents, and other additives [1–3]. The problem is also applicable to subjects ranging from catalysis, in which highly dispersed atom clusters are desired for catalytic activity [4], to lithium-ion batteries [5], in which dendrite growth can lead to device failure. We focus on the deposition of palladium from polyvinylpyrollidone-stabilized palladium nitrate solution [1,2,6]. Palladium is a widely studied system due to its high activity in redox catalysis [7], and much is known about the chemistry of reducing palladium salts [8,9]. Palladium cubes, octahedra, and flowers can be grown [10,11]. There are also many studies of palladium alloys with wide-ranging applications in catalysis [12,13]. We compare the palladium morphology that results from electrochemical deposition both in the presence and absence of ascorbic acid with that of chemical reduction using ascorbic acid.

There are different approaches to *in-situ* liquid cell experiments in Transmission Electron Microscopy (TEM). Because performing electrochemistry in the TEM requires a liquid cell with electrically isolated electrodes, we choose to use a commercial liquid cell TEM holder with this capability. On the other hand, graphene liquid cells offer the benefits of relatively thin liquid layers and window thickness to maximize imaging resolution at the expense of consistent sample preparation and robust electrochemistry capabilities [14,15]. Compared to graphene liquid cells, commercial liquid cells tend to have a worse spatial resolution [16]; however, while 2D materials could be promising as electrode materials [17], graphene liquid cells, for example, are difficult to integrate with electrochemical capabilities. Liquid cell TEM is also possible using an environmental TEM [18]. We use microfabricated chips with electron-transparent SiN_x windows and electrodes capable of

* Corresponding author.
** Corresponding author.
E-mail addresses: acmeng@missouri.edu (A.C. Meng), stach@seas.upenn.edu (E.A. Stach).

https://doi.org/10.1016/j.mtnano.2022.100266
2588-8420/

carrying out electrochemistry in the flow channel. Although the windows bulge due to the presence of liquid in the cell, this can be mitigated to a large extent by *in-situ* bubble formation through water splitting [19]. Thus, *in-situ* bubble generation is used to investigate the initial stages of chemical reduction, in which palladium nanoparticles on the order of a nanometer are formed. Real-time spatially resolved structural characterization of changes in the palladium nucleation and growth as a function of the driving force illustrates the power of liquid cell scanning transmission electron microscopy as an analytical tool.

Recent work using liquid cell TEM has investigated the growth mechanism for Pd during electrodeposition [20,21]. There have also been many studies of nanoparticle growth using liquid cell TEM through chemical or electron beam-induced reduction [5,22–26]. Galvanic replacement reactions have also been studied using *in-situ* liquid cell TEM [13]. We combine a commercially available TEM liquid cell with robust electrochemistry capabilities with *in-situ* bubble generation for improved image signal-to-noise ratio to systematically test the differences between electrochemical, chemical, and electron beam-induced growth. Because electrochemical and chemical processing occurs at real time in the TEM, we can observe the differences in Pd morphology due to changes in the driving force.

2. Materials and methods

TEM characterization was performed in a JEOL JEM-F200 Scanning/Transmission Electron Microscope (S/TEM) equipped with two large-area silicon drift detectors (SDD) with 1.7 steradian solid angle for energy dispersive X-ray spectroscopy (EDS) measurements. For STEM imaging, probe size 7 was used with a 40 μm condenser aperture, yielding approximately 60 pA probe current. For liquid cell experiments, a type II liquid cell TEM holder (Hummingbird Scientific) was used with an airtight 1000 μL syringe and syringe pump. Type P5 liquid cell chips with Pt electrodes and 250 nm spacer chips (Hummingbird Scientific) were plasma cleaned in Ar for 1 min at a forward transmitted power of 40 W prior to sample loading to facilitate liquid filling the cell. The liquid cell was primed with 0.02–0.03 wt% $Pd(NO_3)_2$ solution stabilized with 40 kDa polyvinylpyrrolidone (referred to as Pd-PVP herein) prior to insertion into the TEM for all experiments. To investigate the effect of ascorbic acid chemical reductant, immediately prior to the experiment, a 1:1 mixture of freshly mixed liquid (1:1::0.03 wt % Pd-PVP:0.01 M ascorbic acid, v/v) was primed up to a manual valve at the liquid entrance port of the TEM holder. There is a 20 μL dead volume between the manual valve and the sample chip, which is traversed in a minute at a 20 μL/min flow rate. We begin characterization of chemical reduction approximately 2 min after flowing the freshly mixed liquid at 20 μL/min to ensure that the chemical reductant is present. All STEM images collected are from *in-situ* experiments, and the video files are included in the Supporting Information. Electrochemical measurements were performed using a BioLogic SP-200 potentiostat. *In-situ* in the TEM, Pt working, counter, and reference electrodes are used; *ex-situ*, graphite rod working and counter electrodes are used, and a Pt foil reference electrode is used.

Supplementary video related to this article can be found at https://doi.org/10.1016/j.mtnano.2022.100266

3. Results

First, we observe 3 wt% Pd-PVP solution in the liquid cell with no driving force for reduction, either electrochemical or chemical. This is to verify the absence of significant sedimentation or aggregate formation in the solution. At low magnifications, the STEM image is featureless aside from the electrodes (Fig. 1a). However, although an initial higher-magnification STEM image also shows no features aside from an electrode (Fig. 1b), deposits begin to form gradually at high magnifications. The observation of square-shaped contrast coinciding with the field of view at high magnifications is consistent with electron beam-induced reduction of the Pd-PVP solution. Also, spot-shaped deposits form at the top left corner of the field of view because the beam position resets to begin the next scan. To verify that the deposits are Pd, water splitting is used to form a bubble *in-situ*, and EDS mapping is performed on a deposit and a nearby region. The spectra show that the deposited material is Pd, and that surrounding regions do not have Pd (Fig. 1f and g). We note that deposits continue to form after a bubble is formed due to a thin film of liquid being present.

To observe electrochemical reduction of the Pd-PVP, 0.03 wt% Pd-PVP solution is reduced *in-situ* in the liquid cell under full liquid conditions by passing −10 nA of current through the working electrode under galvanostatic conditions. Pd dendrites begin growing immediately after reduction begins, consistent with diffusion-limited growth. The dendrites grow until they extend approximately 2 μm away from the working electrode, and the average dendrite width is 52 ± 13 nm (Fig. 2b and c). Video of electrochemical reduction is provided in the Supporting Information. Growth slows as the dendrites are limited by the dimensions of the liquid cell and the proximity of the counter and reference electrodes to the working electrode. Post electrodeposition, a bubble was generated using *in-situ* water splitting in order to perform EDS mapping of the dendrite (Fig. 2d–f).

In contrast, chemical reduction of the Pd-PVP is observed by flowing a 1:1 v/v mixture of 0.03 wt% Pd-PVP and 0.01 M ascorbic acid. Under full liquid conditions, we were surprised to see no Pd crystals growing. There were a couple of large Pd aggregates observed, but these did not change significantly over time. An aggregate was EDS mapped in full liquid conditions to confirm the presence of Pd (Fig. 3a and b). Because we were anticipating significantly smaller Pd nanoparticles, a bubble was generated to improve the STEM image intensity signal-to-noise ratio. Post bubble formation, small Pd nanoparticles are observed to result (diameter = 6 ± 1 nm) due to chemical reduction (Fig. 3c). The nanoparticles are very closely spaced and have similar particle sizes; the structure is significantly more isotropic compared to the electrodeposited Pd. EDS mapping confirms that these small particles are indeed Pd (Fig. 3c–e). At lower magnification, slightly larger Pd particles are also observed (diameter = 18 ± 3 nm) (Fig. 3e). The chemical reduction process is captured on video as well (See Supporting Information).

The effect of ascorbic acid on electrochemical reduction of the Pd-PVP solution was examined by flowing freshly mixed 1:1 0.03 wt% Pd-PVP/0.01 M ascorbic acid into the cell and then flowing −10 nA of current through the working electrode under galvanostatic conditions. The structure of the Pd crystals that grow is significantly more compact, forming a dense thin film surrounding the working electrode as observed under full liquid conditions (Fig. 4a–c). While there are some dendrites at the surface of this film, the branches are significantly thicker and have less space in between. Video of the combined electrochemical and chemical reduction is provided in the Supporting Information. EDS mapping is also performed after *in-situ* bubble formation and confirms the presence of Pd (Fig. 4d–f). Due to the presence of ascorbic acid, away from the electrodes, chemical reduction also occurs, resulting in Pd crystals similar to those shown in Fig. 3c–e.

Finally, the electrochemical experiments are repeated on the bench. For galvanostatic reduction without ascorbic acid, we observe that using a fixed reductive current, the working electrode

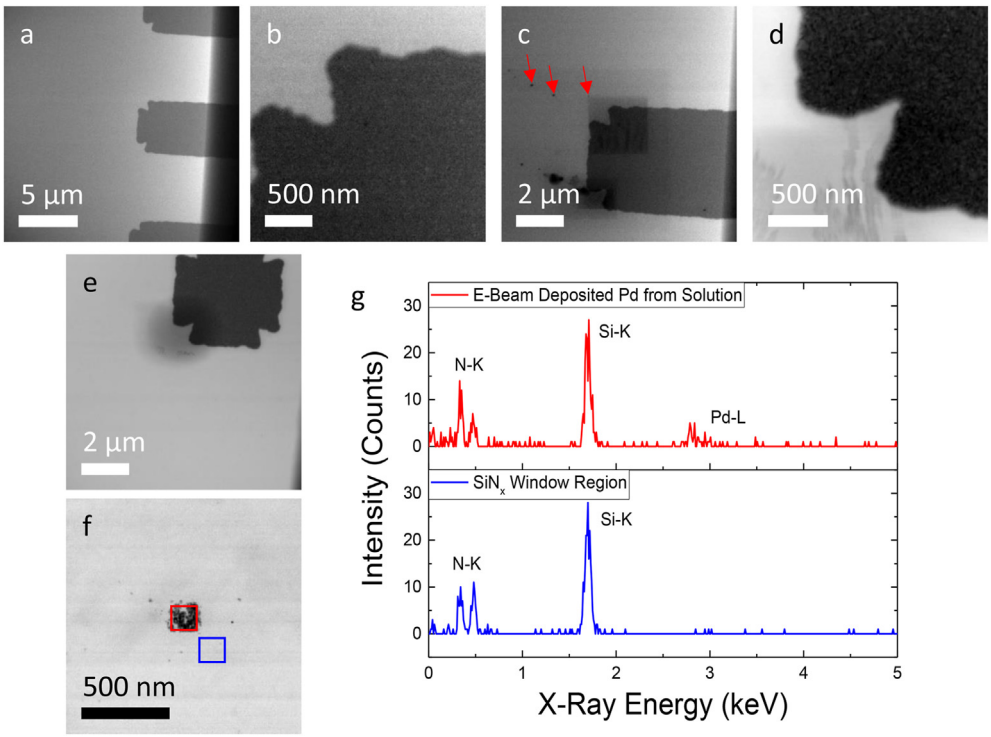

Fig. 1. BF-STEM images of electron beam-induced reduction of $Pd(NO_3)_2$-PVP: a) low-magnification BF STEM of electrodes and SiN_x window region, b) high-magnification BF STEM of working electrode, and c) beam-induced Pd deposition under full liquid conditions; characterization of electron beam-induced Pd deposition under thin liquid conditions (d–g): d) high-magnification and e) subsequent low-magnification BF STEM of beam-induced deposition; f) Pd square deposited by prolonged electron beam exposure and g) EDS spectra from outlined regions in c).

potential becomes slightly more positive in the *in-situ* experiment whereas the working electrode potential becomes more negative and reaches a plateau in the *ex-situ* experiment (Fig. 5a, c). For galvanostatic reduction with ascorbic acid, we observe that at a fixed reductive current, the working electrode potential becomes more positive in the *in-situ* experiment; in the *ex-situ* experiment at lower current densities, the working electrode potential behaves similarly to reduction without ascorbic acid, however, at higher current densities, the working electrode potential also becomes more positive, reflecting the *in-situ* experiment.

Cyclic voltammetry is also performed *ex-situ*. Without ascorbic acid, reductive current begins to flow when the working electrode potential is just below 1 V. Assuming the reference electrode is close to the standard hydrogen electrode, this would be close to the reduction potential of Pd^{2+}, which is 0.915 V vs. SHE. This is similarly the case when ascorbic acid is present. Introducing ascorbic

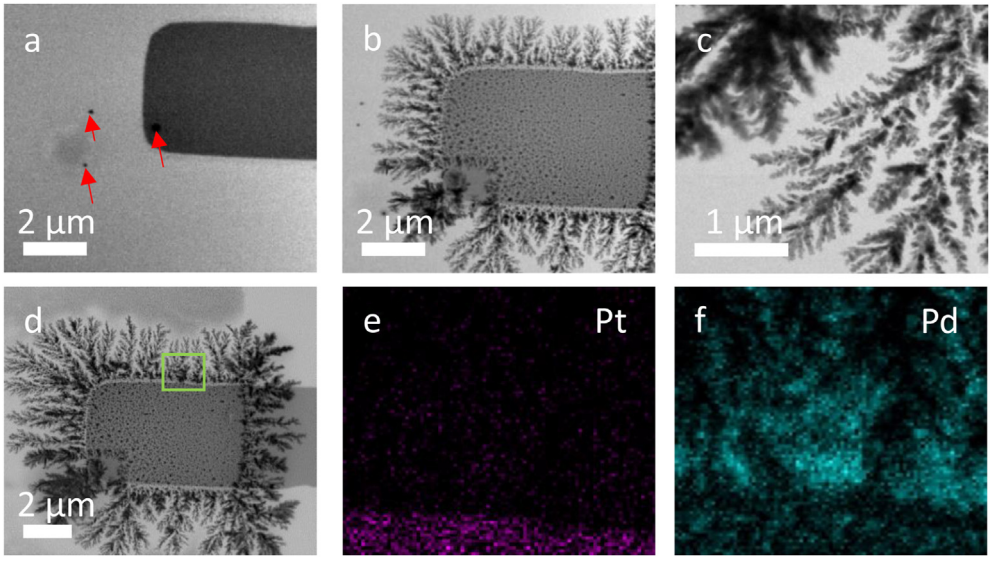

Fig. 2. BF STEM image of electrochemical reduction of $Pd(NO_3)_2$-PVP under full liquid conditions: a) before growth, b) after electrodeposition, and c) showing dendrite structure; d) BF STEM image and EDS maps of the e) Pt and f) Pd signals from the green rectangle in d) under thin liquid conditions.

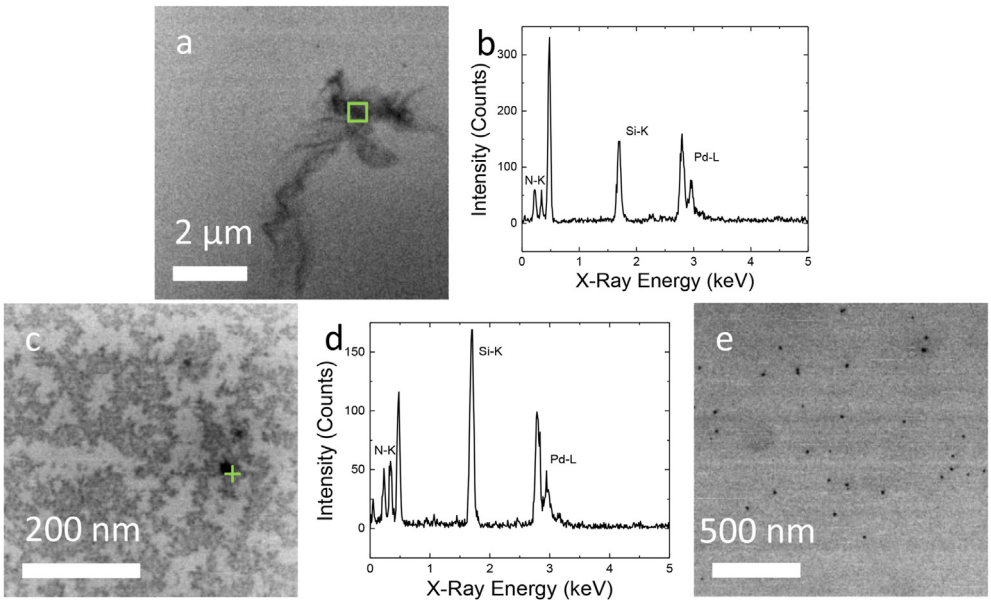

Fig. 3. a) BF STEM image and b) corresponding EDS spectrum of chemically reduced Pd under full liquid conditions; c) BF STEM image and d) corresponding EDS spectrum and e) lower-magnification BF STEM image of chemically reduced Pd under thin liquid conditions.

acid into the solution results in an onset for additional reductive current at approximately −0.3 V. This is consistent with the reduction potentials of ascorbate under acidic conditions [27].

4. Discussion

The convoluting effects of the electron beam are one of the main challenges in *in-situ* TEM experiments. While lattice imaging under liquid conditions with probe aberration correction is possible by generating a bubble *in-situ* in the liquid cell [19], observation of the Pd-PVP solution shows that beam-induced reduction at higher magnifications influences the sample as the image is collected. Technically, all *in-situ* Pd-PVP growth experiments involve some amount of electron beam-induced reduction. However, as this cannot be entirely removed from the experiment, the control experiment shows that beam effects are only dominant at higher magnifications. Fig. 2b–d shows the influence of electron beam-induced Pd reduction on Pd electrodeposition. The region at the bottom left of Fig. 2b and d shows significantly thicker dendrite structures. These thicker dendrites formed due to focusing the beam at high magnification for the image taken in Fig. 2c. The effect of the electron beam is similar to the effect of a chemical reductant

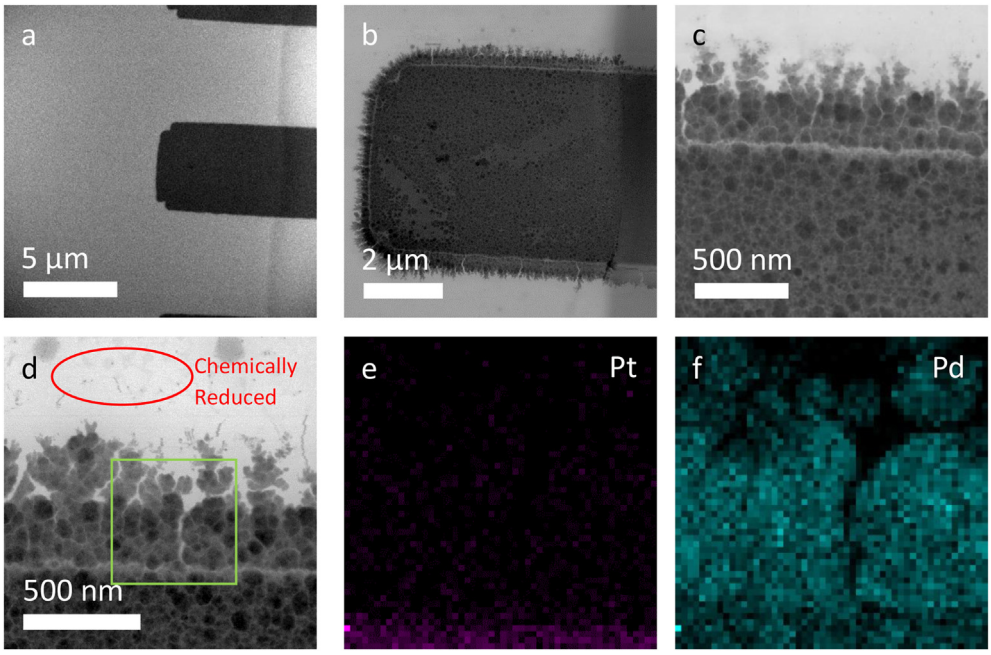

Fig. 4. BF STEM image of electrochemical reduction of $Pd(NO_3)_2$-PVP in the presence of L-ascorbic acid under full liquid conditions: a) before growth, b) after electrodeposition, and c) showing dendrite structure; d) BF STEM image and EDS maps of e) Pt and f) Pd under thin liquid conditions.

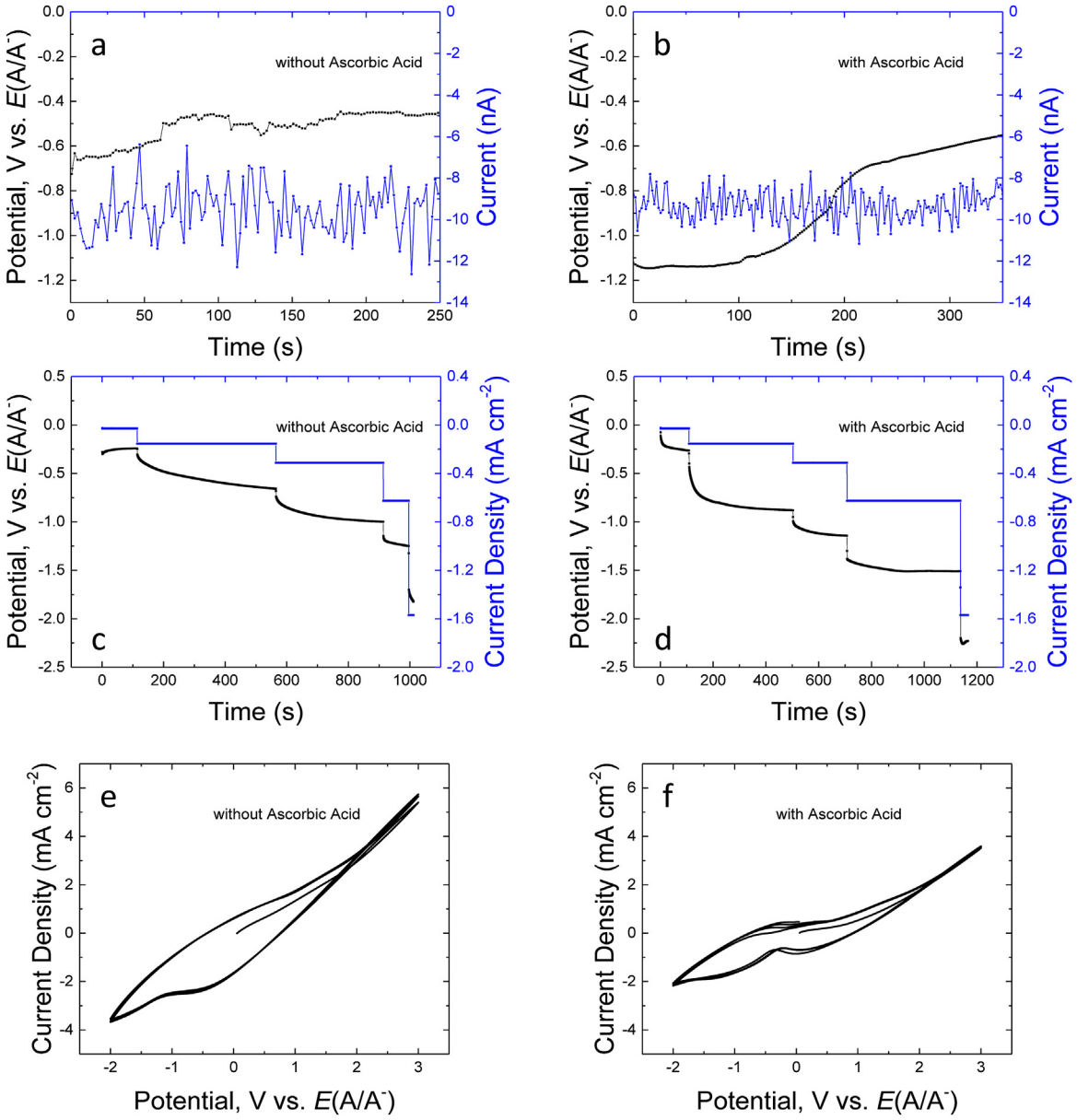

Fig. 5. *In-situ* chronopotentiometry data from deposition in the TEM a) without ascorbic acid, and b) with ascorbic acid. Benchtop cyclic voltammetry c) without ascorbic acid, d) with ascorbic acid and chronopotentiometry, and e) without ascorbic acid, and f) with ascorbic acid.

in reducing the space between dendrites, except that it is spatially localized to the beam. At low magnifications, with the addition of either a chemical or electrochemical driving force, beam effects no longer play a dominant role in growth. Another concern involves adequate flow to the liquid cell: replenishing chemical species to the region being imaged is important due to effects of mass transport limitations. At a flow rate of 20 μL/min and a cell volume of the electron-transparent region (90 μm × 600 μm × 250 nm) on the order of 10^{-5} μL, there are more than 10^6 volume changes per minute. Chemical species replenishment is not expected to be limiting mass transport as a result.

To minimize the effects of the electron beam on the *in-situ* electrochemistry, galvanostatic experiments were chosen to fix the current at the electrodes. This prevents drift in electrochemical potential due to the electron microscope from unduly affecting the experiment. The *in-situ* experiments were compared to *ex-situ* experiments under the same conditions. Cyclic voltammetry was only performed *ex-situ*; while we have demonstrated cylic voltammetry *in-situ* [19], here we focus on the differences in driving force for Pd crystallization.

One interesting observation is that chemical reduction of Pd results in very small nanoparticle aggregates that form more dense deposits as opposed to electrochemical reduction, which results in significantly larger dendrite structures that branch out. We attribute this difference to mass transport limitation of the palladium salt during electrodeposition, which can deplete the solution near the electrodes. This is consistent with the observed dendrite structure. During chemical reduction, the ascorbic acid reductant concentration is uniform and in significant excess, consistent with the observed compact film structure. It is expected that crystalline fcc Pd growth results from either electrochemical or chemical reduction. Electrodeposited Pd has been shown to be fcc [28], similar to Pd reduced from PVP-stabilized solutions [2]. While spatially resolved electron diffraction (e.g., 4D-STEM) could be used

to differentiate between electrodeposited and chemically reduced Pd, there are some complications arising from beam-induced reduction. Whereas electrochemical reduction of $Pd(NO_3)_2$-PVP without ascorbic acid led to dendrite structures, chemical reduction in ascorbic acid led to approximately uniformly sized particles on the nanometer scale that are very closely spaced. Using liquid cell TEM and *in-situ* bubble formation, both processes are observed in real time at the relevant length scales. In particular, chemical reduction of $Pd(NO_3)_2$-PVP is observed at the nanometer scale, giving a glimpse of the early stages of growth following nucleation. While the structures of Pd crystallites that result are well known, these experiments illustrate the power of liquid cell TEM for mechanistic studies of crystal growth from electrochemical and chemical reduction processes. Furthermore, we show that the presence of ascorbic acid during electrochemical reduction of $Pd(NO_3)_2$-PVP results in growth of a more compact film instead of dendrite structures. Note that this occurs in spite of the fact that the $Pd(NO_3)_2$ concentration is a factor of two lower for electrochemical reduction with ascorbic acid that than in the case without. Given that poor mass transport tends to drive the formation of dendrites, this data suggests that the presence of ascorbic acid promotes increased nucleation of Pd in the regions in between dendrites, resulting in the observed film structure.

5. Conclusion

We varied the driving force for Pd crystal growth from $Pd(NO_3)_2$-PVP from electrochemical to chemical to a combination of both and used liquid cell TEM at nanoscale resolution to observe the structural changes during growth. The high resolution necessary for characterization of nanometer-sized particles formed during chemical reduction was achieved by employing *in-situ* water splitting, a robust method for reducing the thickness of the liquid in the cell. Pd dendrites were grown using electrochemical deposition in the absence of chemical reductant, Pd nanoparticles were obtained through reduction by ascorbic acid, and Pd thin film was grown using electrochemical deposition in the presence of ascorbic acid. Because electrochemical data and structural information can be collected in real time, liquid cell TEM can also be used when multiple species are being simultaneously reduced; this has applications in understanding the growth of alloys, for example.

CRediT author statement

Andrew C. Meng: conceptualization, methodology, investigation, data curation, visualization, formal analysis, writing – original draft, writing – review and editing. **Rui Serra-Maia**: investigation, data curation, writing – review and editing. **Ke-Bin Low**: conceptualization, methodology, writing – review and editing. **Huifang Lang**: methodology, writing – review and editing. **Eric A. Stach**: conceptualization, methodology, formal analysis, writing – review and editing, supervision, funding acquisition.

Data availability

The authors confirm that the data supporting the findings of this study are available within the article and its supplementary materials.

Declaration of competing interest

The authors declare that they have no known competing financial interests or personal relationships that could have appeared to influence the work reported in this paper.

One author, Eric Stach, has an equity interest in Hummingbird Scientific. Instrumentation from Hummingbird Scientific is used in this study.

Acknowledgments

The authors acknowledge funding from BASF. This work was carried out in part at the Singh Center for Nanotechnology, which is supported by the NSF National Nanotechnology Coordinated Infrastructure Program under grant NNCI-1542153. Transmission electron microscopy was performed in facilities supported by the NSF MRSEC Program under Award No. DMR-1720530.

References

[1] S.C. Jung, Y.-K. Park, H.-Y. Jung, S.C. Kim, Effect of stabilizing agents on the synthesis of palladium nanoparticles, J. Nanosci. Nanotechnol. 17 (4) (2017) 2833–2836.
[2] K. Walbrück, F. Kuellmer, S. Witzleben, K. Guenther, Synthesis and characterization of PVP-stabilized palladium nanoparticles by XRD, SAXS, SP-ICP-MS, and SEM, J. Nanomater. 2019 (2019), 4758108.
[3] E. Higuchi, M. Kawai, M. Chiku, H. Inoue, Synthesis and electrochemical characterization of palladium crystals enclosed by (100) facets by seed-mediated fabrication, Int. J. Electrochem. 2018 (2018), 7138638.
[4] Y. Wang, A. Biby, Z. Xi, B. Liu, Q. Rao, X. Xia, One-pot synthesis of single-crystal palladium nanoparticles with controllable sizes for applications in catalysis and biomedicine, ACS Appl. Nano Mater. 2 (7) (2019) 4605–4612.
[5] M.R. Hauwiller, X. Zhang, W.-I. Liang, C.-H. Chiu, Q. Zhang, W. Zheng, C. Ophus, E.M. Chan, C. Czarnik, M. Pan, F.M. Ross, W.-W. Wu, Y.-H. Chu, M. Asta, P.W. Voorhees, A.P. Alivisatos, H. Zheng, Dynamics of nanoscale dendrite formation in solution growth revealed through in situ liquid cell electron microscopy, Nano Lett. 18 (10) (2018) 6427–6433.
[6] V.L. Nguyen, D.C. Nguyen, H. Hirata, M. Ohtaki, T. Hayakawa, M. Nogami, Chemical synthesis and characterization of palladium nanoparticles, Adv. Nat. Sci. Nanosci. Nanotechnol. 1 (3) (2010), 035012.
[7] A.C. Meng, K.-B. Low, A.C. Foucher, Y. Li, I. Petrovic, E.A. Stach, Anomalous metal vaporization from Pt/Pd/Al2O3 under redox conditions, Nanoscale 13 (26) (2021) 11427–11438.
[8] J. Liu, F. He, T.M. Gunn, D. Zhao, C.B. Roberts, Precise seed-mediated growth and size-controlled synthesis of palladium nanoparticles using a green chemistry approach, Langmuir 25 (12) (2009) 7116–7128.
[9] M. Luty-Błocho, M. Wojnicki, G. Włoch, K. Fitzner, Green method for efficient PdNPs deposition on carbon carrier in the microreactor system, J Nanopart Res 20 (9) (2018) 239, 239.
[10] A. Chen, C. Ostrom, Palladium-based nanomaterials: synthesis and electrochemical applications, Chem. Rev. 115 (21) (2015) 11999–12044.
[11] Y. Sun, L. Zhang, H. Zhou, Y. Zhu, E. Sutter, Y. Ji, M.H. Rafailovich, J.C. Sokolov, Seedless and templateless synthesis of rectangular palladium nanoparticles, Chem. Mater. 19 (8) (2007) 2065–2070.
[12] K.L. Jungjohann, S. Bliznakov, P.W. Sutter, E.A. Stach, E.A. Sutter, In situ liquid cell electron microscopy of the solution growth of Au–Pd core–shell nanostructures, Nano Lett. 13 (6) (2013) 2964–2970.
[13] E. Sutter, K. Jungjohann, S. Bliznakov, A. Courty, E. Maisonhaute, S. Tenney, P. Sutter, In situ liquid-cell electron microscopy of silver–palladium galvanic replacement reactions on silver nanoparticles, Nat. Commun. 5 (1) (2014) 4946.
[14] J.R. Jokisaari, X. Hu, A. Mukherjee, V. Uskoković, R.F. Klie, Hydroxyapatite as a scavenger of reactive radiolysis species in graphene liquid cells for in situ electron microscopy, Nanotechnology 32 (48) (2021), 485707.
[15] C. Wang, Q. Qiao, T. Shokuhfar, R.F. Klie, High-resolution electron microscopy and spectroscopy of ferritin in biocompatible graphene liquid cells and graphene sandwiches, Adv. Mater. 26 (21) (2014) 3410–3414.
[16] J.M. Yuk, J. Park, P. Ercius, K. Kim, D.J. Hellebusch, M.F. Crommie, J.Y. Lee, A. Zettl, A.P. Alivisatos, High-resolution EM of colloidal nanocrystal growth using graphene liquid cells, Science 336 (6077) (2012) 61–64.
[17] S.F. Tan, K. Reidy, S. Lee, J. Klein, N.M. Schneider, H.Y. Lee, F.M. Ross, Multilayer graphene—a promising electrode material in liquid cell electrochemistry, Adv. Funct. Mater. 31 (46) (2021), 2104628.
[18] B.D.A. Levin, D. Haiber, Q. Liu, P.A. Crozier, An open-cell environmental transmission electron microscopy technique for in situ characterization of samples in aqueous liquid solutions, Microsc. Microanal. 26 (1) (2020) 134–138.
[19] R. Serra-Maia, P. Kumar, A.C. Meng, A.C. Foucher, Y. Kang, K. Karki, D. Jariwala, E.A. Stach, Nanoscale chemical and structural analysis during in situ scanning/transmission electron microscopy in liquids, ACS Nano 15 (6) (2021) 10228–10240.
[20] J. Yang, C.M. Andrei, Y. Chan, B.L. Mehdi, N.D. Browning, G.A. Botton, L. Soleymani, Liquid cell transmission electron microscopy sheds light on the mechanism of palladium electrodeposition, Langmuir 35 (4) (2019) 862–869.

[21] J. Yang, S. Prabhudev, C.M. Andrei, G.A. Botton, L. Soleymani, Deposition and morphological evolution of nanostructured palladium during potential cycling: a liquid-cell TEM study, Chem. Comm. 55 (62) (2019) 9204–9207.
[22] M.H. Nielsen, D. Li, H. Zhang, S. Aloni, T.Y.-J. Han, C. Frandsen, J. Seto, J.F. Banfield, H. Cölfen, J.J. De Yoreo, Investigating processes of nanocrystal formation and transformation via liquid cell TEM, Microsc. Microanal. 20 (2) (2014) 425–436.
[23] A. De Clercq, W. Dachraoui, O. Margeat, K. Pelzer, C.R. Henry, S. Giorgio, Growth of Pt–Pd nanoparticles studied in situ by HRTEM in a liquid cell, J. Phys. Chem. Lett. 5 (12) (2014) 2126–2130.
[24] H.-G. Liao, H. Zheng, Liquid cell transmission electron microscopy study of platinum iron nanocrystal growth and shape evolution, J. Am. Chem. Soc. 135 (13) (2013) 5038–5043.
[25] T.J. Woehl, T. Moser, J.E. Evans, F.M. Ross, Electron-beam-driven chemical processes during liquid phase transmission electron microscopy, MRS Bull. 45 (9) (2020) 746–753.
[26] W. Gao, A.O. Elnabawy, Z.D. Hood, Y. Shi, X. Wang, L.T. Roling, X. Pan, M. Mavrikakis, Y. Xia, M. Chi, Atomistic insights into the nucleation and growth of platinum on palladium nanocrystals, Nat. Commun. 12 (1) (2021) 3215.
[27] H. Borsook, G. Keighley, Oxidation-reduction potential of ascorbic acid (vitamin C), Proc. Natl. Acad. Sci. U.S.A. 19 (9) (1933) 875.
[28] M. Rezaei, S.H. Tabaian, D.F. Haghshenas, The role of electrodeposited Pd catalyst loading on the mechanisms of formic acid electro-oxidation, Electrocatalysis 5 (2) (2014) 193–203.